

Essential Bicycle Dynamics for Microscopic Traffic Simulation: An Example Using the Social Force Model

Schmidt, C.M.; Dabiri, A.; Schulte, F.; Happee, R.; Moore, J.K.

DOI

[10.59490/65a5124da90ad4aecf0ab147](https://doi.org/10.59490/65a5124da90ad4aecf0ab147)

Publication date

2024

Document Version

Final published version

Published in

Proceedings of the 5th Symposium on the Dynamics and Control of Single-track Vehicles

Citation (APA)

Schmidt, C. M., Dabiri, A., Schulte, F., Happee, R., & Moore, J. K. (2024). Essential Bicycle Dynamics for Microscopic Traffic Simulation: An Example Using the Social Force Model. In J. Moore, E. de Vries, A. Dressel, & L. Alizadehsarav (Eds.), *Proceedings of the 5th Symposium on the Dynamics and Control of Single-track Vehicles: Bicycle and Motorcycle Dynamics 2023, October 18-20, Delft, The Netherlands* (The Evolving Scholar; Vol. 3). TU Delft OPEN Publishing. <https://doi.org/10.59490/65a5124da90ad4aecf0ab147>

Important note

To cite this publication, please use the final published version (if applicable). Please check the document version above.

Copyright

Other than for strictly personal use, it is not permitted to download, forward or distribute the text or part of it, without the consent of the author(s) and/or copyright holder(s), unless the work is under an open content license such as Creative Commons.

Takedown policy

Please contact us and provide details if you believe this document breaches copyrights. We will remove access to the work immediately and investigate your claim.

Type of the Paper: Conference Paper

Revised

Essential Bicycle Dynamics for Microscopic Traffic Simulation: An Example Using the Social Force Model

[version 2; peer reviewed]

Christoph M. Schmidt^{1,*}, Azita Dabiri¹, Frederik Schulte¹, Riender Happee¹, Jason K. Moore¹

¹ Delft University of Technology, The Netherlands; c.m.schmidt@tudelft.nl, ORCID 0000-0002-9405-6384, a.dabiri@tudelft.nl, ORCID 0000-0002-1296-7580, f.schulte@tudelft.nl, ORCID 0000-0003-3159-4393, r.happee@tudelft.nl, ORCID 0000-0001-5878-3472, j.k.moore@tudelft.nl, ORCID 0000-0002-8698-6143

* corresponding author

Name of Editor: Edwin De Vries

First published: 22/09/2023

Last published: 07/05/2024

Citation: Schmidt, C., Dabiri, A., Schulte, F., Happee, R. & Moore, J. (2024). Essential Bicycle Dynamics for Microscopic Traffic Simulation: An Example Using the Social Force Model [version 2; peer reviewed]. The Evolving Scholar - BMD 2023, 5th Edition.

This work is licensed under a Creative Commons Attribution License (CC-BY).

Abstract:

Microscopic simulation is an established tool in traffic engineering and research in which aggregated traffic performance measures are inferred from the simulation of individual agents. Measures describing the safety and efficiency of road user interactions gain importance for recent developments such as automated vehicles and urban cycling. However, current simulation frameworks model interactions including cyclists without considering the constraints of two-wheeler dynamics (mechanics of a bicycle in motion) that limit feasible maneuvers in a cycling conflict. To address this issue, we propose to bring bicycle dynamics to traffic simulation. We demonstrate that a novel reformulation of the social force framework can create input signals for a controlled inverted pendulum bicycle model and thereby enable more realistic two-dimensional open space simulation of cyclist interactions. The inverted pendulum model introduces the need to stabilize the bicycle as a constraint to the reactive behavior of simulated cyclists. Furthermore, it enables the simulation of countersteering and weaving for stabilization. Our cyclist social forces have anisotropic force fields with respect to relative interaction position and orientation to describe the varying interaction constellations in open space. With these models, we simulate the yaw angle step response and four test cases with up to three cyclists to show that the generated trajectories notably differ from results obtained from a 2D bicycle model without roll angle simulation. Measurements of the maximum lateral path deviation and post-encroachment time show that these differences are relevant for typical applications. Our work demonstrates the potential of introducing physics-based bicycle dynamics to the microscopic simulation of individual road user interactions and the fundamental capability of our reformulated cyclist social forces to do so. Going further, we plan to calibrate and validate our model based on naturalistic cycling data to support the initial results of this work.

Keywords:

Social Force Model, Microscopic Traffic Simulation, Cyclist Behaviour, Bicycle Dynamics, Bicycle Trajectories

Introduction

In traffic engineering and research, microscopic traffic simulation is a widespread tool to assess the impact of innovations in traffic control, road infrastructure, connectivity, automation, and other fields. Researchers and practitioners measure performance indicators for traffic efficiency and safety from the movements of individually simulated road users. Historically designed for cars, microscopic simulations use lane-based architectures, where lateral motion is limited to placement on the lane without considering vehicle dynamics. With this architecture, simulation environments struggle to accurately describe cyclists and their diverse motion patterns. Compared to cars, cyclists show less lane discipline and utilize legal and illegal options for the available infrastructure.

Previously, researchers have investigated several approaches to capture cycling behavior into models suitable for microscopic simulation. Kathis et al. (2021) and Kurtc and Treiber (2020) evaluate the adaptation of car-following models to bicycle behavior. While these successfully model some aggregated longitudinal characteristics, they do not capture the two-dimensional motion encountered in intersections and do not sufficiently enable lateral evasive maneuvers in conflicts. Popular approaches to enable two-dimensional motion are cyclist adaptations of the pedestrian social force model (Helbing and Molnár, 1995). In this paradigm, imaginary forces describe a person's motivation to act. Attractive forces draw road users to their intended destination, while repulsive forces prevent collisions with their environment. To capture the constraints of two-wheeler motion, researchers separate the social force acting on a cyclist into lateral and longitudinal components (Kathis, 2023). Other researchers improve the cycling characteristics by adding path-planning modules (Rinke et al., 2017) or anisotropic characteristics to the repulsive force fields of other road users (Yuan et al., 2019; Dias et al., 2018). Lastly, researchers add complex tactical layers to the social force model that explicitly model different behaviors and preferences depending on a cyclist's surroundings (Ni et al., 2023; Liang et al., 2018; Rinke et al., 2017). While all these innovations improve the capabilities of the social force model to simulate bicycling, we have not found work that introduces the physical constraints of riding a two-wheeled bicycle into the framework.

The inclusion of two-wheeler vehicle dynamics must consider two effects. Firstly, cyclists cannot accelerate laterally without longitudinal motion and steering. Direct lateral acceleration, however, is possible with the particle dynamics of the original pedestrian social force models. For cars, Huang et al. (2012) use the social force as input to a simple vehicle dynamics model to prevent unrealistic lateral acceleration. A similar application to bicycles is currently missing. Secondly, cyclists do not only steer to reach a destination but simultaneously need to stabilize the bicycle. This limits the set of feasible reactions without falling and thus impacts how cyclists react to their environment. One relevant effect is oscillating during stabilization. After disturbance or at low speeds, cyclist trajectories show lateral motions resulting from pedaling frequencies and stabilizing the bike. Another effect is countersteering, which requires cyclists to momentarily steer in the opposite direction of an intended turn to initiate an inward roll angle.

The simulation of safety is of increasing interest, specifically for cyclists and new forms of mobility like automated vehicles. For this, models must describe conflict mechanisms (Arun et al., 2021). The aforementioned effects directly impact the formation and development of cycling conflicts. For example, the need to countersteer limits feasible reaction times and amplitudes if a sudden evasive maneuver is required. Or, an overtaking car might collide with a cyclist when a temporal loss of stability requires weaving. Existing simulation frameworks do not consider these effects and thus do not sufficiently capture the causality of road user interactions. We propose to add physics-based road user models to microscopic simulation and hypothesize that this enables the creation of more meaningful conflicts in traffic simulation by improving the simulated causal chain of events. In an ongoing project, we are developing a cyclist social force model with realistic bicycle dynamics to validate this hypothesis. The present paper presents our first results of a reformulated social force coupled with controlled vehicle dynamic models. We use an inverted pendulum bicycle model, which enables us to simulate the countersteering effect, stabilizing oscillation, and minimum stable speeds. Similarly to Dias et al. (2018), we introduce a new version of anisotropic repulsive force fields depending on the relative position and relative orientation between cyclists. Additionally, we propose spline-based trajectory planning to calculate the destination force. Without loss of generality, we limit the scope of this paper to bicycle-bicycle interactions and do not yet consider repulsive forces from infrastructure boundaries. For a complete model, these components may be added in the future. We demonstrate the qualitative functionality of our approach with four different generic scenarios and discuss apparent benefits and shortcomings. Promising results pave the way for further development and full validation of a cyclist social force model that creates realistic safety-sensitive microscopic road user interactions. A software implementation of our model including experiments and all parameter values of this paper is available at <https://github.com/chrismo-schmidt/cyclistsocialforce>.

The remainder is structured as follows. First, we introduce the dynamic bicycle model, the cyclist social force model, and the control architecture. Then, we apply our model to four exemplary scenarios. Finally, we discuss the benefits and shortcomings of the results.

Method

To introduce realistic bicycle physics into the microscopic simulation, we add a bicycle dynamics model to the social force model. Figure 1 shows an overview of the proposed simulation system architecture. Following Kathis (2023), the magnitude and angle of the social force vectors are separated. In our architecture, individual dynamic models for speed and yaw then have the angle or magnitude as input and the updated bicycle state as output. Both models share the same state $z = (x, y, v, \psi, \theta)^T$. The following subsections explain the model building blocks in detail.

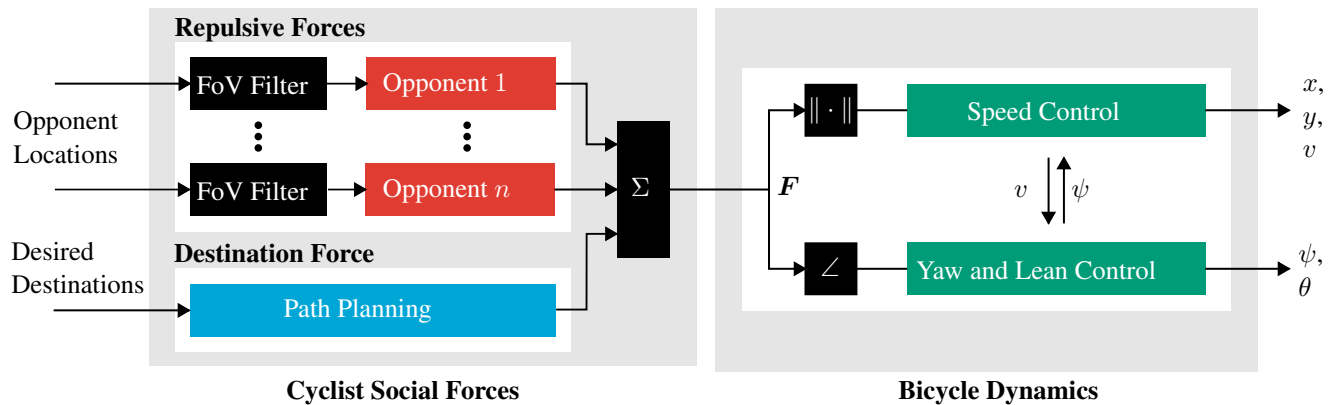


Figure 1. System overview of a cyclist with n opponents, experiencing the aggregated social forces F and controlling their speed v and yaw angle ψ accordingly. This also results in the bike’s position x, y and roll angle θ .

Dynamic Bicycle Model

For our approach, we choose the linear inverted pendulum bicycle model (Karnopp, 2013, ch. 7). This simple model captures the desired effects of bicycle dynamics with minimal complexity. As a first approach for micro-simulation, we deem more complex effects like self-stabilization negligible. Figure 2 shows the inverted pendulum model. Each wheel is modeled as a point in the ground plane that is constrained to prevent relative lateral motion. The front wheel rotates about the vertical axis for steering. The bicycle and rider are modeled as an inverted compound pendulum that can roll about the line connecting the rear and front wheel points. The relative motion of the rider’s body on the bicycle frame is neglected. At a constant longitudinal speed v , steering leads to lateral acceleration, which can be used to stabilize the pendulum.

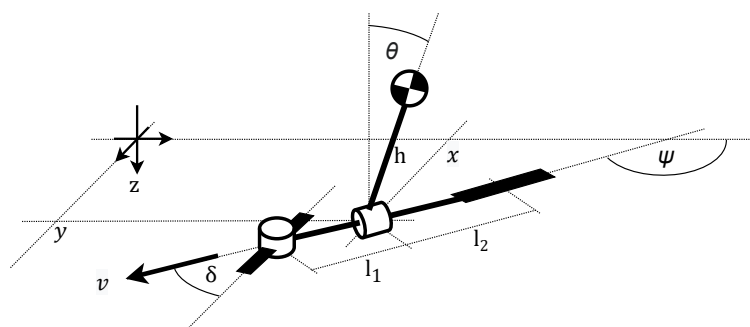


Figure 2. The inverted pendulum bicycle model.

As shown by Karnopp (2013, ch. 7), the transfer function relating the steer angle δ and the roll angle θ is

$$G_{\theta}(s) = \frac{\Theta(s)}{\Delta(s)} = -K \frac{\tau_2 s + 1}{\tau_1^2 s^2 - 1}, \quad (1)$$

with $\tau_1^2 = \frac{I_b + mh^2}{mgh}$, $\tau_2 = \frac{l_2}{v}$, $K = \frac{v^2}{gl}$, and $l = l_1 + l_2$, where I_b is the moment of inertia of the bike and rider around the roll axis, m is the combined mass of rider and bike, and g is the gravitational constant. We modify Karnopp's model by adding inertia and damping to the steering system, capturing the effects of resistance from tire friction and passive arm joint friction. The following transfer function describes dampened steering with the steering torque $T(s)$ as input.

$$G_\delta(s) = \frac{\Delta(s)}{T(s)} = \frac{1}{I_s s^2 + cs}. \quad (2)$$

Here, I_s denotes the moment of inertia of the steering system around the steering axis and c the damping coefficient of the rotational motion. $G_\delta(s)$ is derived from the net torque equilibrium of the rotating steer column. The final yaw angle may be calculated from

$$G_\psi(s) = \frac{\Psi(s)}{\Delta(s)} = \frac{1}{\tau_3 s}, \quad (3)$$

derived from the geometric relationship while using a small angle approximation for δ and $\tau_3 = \frac{l}{v}$ (Moore, 2015).

Cyclist Social Forces

The original pedestrian model describes particles that can move in any direction. A superposition of repulsive and attractive psychosocial forces exerted on the individual by their intentions and environment acts as the driving force (Helbing and Molnár, 1995):

$$\mathbf{F}_a = \mathbf{F}_a^0 + \sum_b \mathbf{F}_{a,b} + \sum_B \mathbf{F}_{a,B} + \sum_i \mathbf{F}_{a,i} \quad (4)$$

Here, $\mathbf{F}_a = \frac{d\mathbf{v}}{dt}$ is the social force experienced by a simulated pedestrian a . \mathbf{F}_a^0 is a social force that pulls a towards the intended destination. $\mathbf{F}_{a,b}$ are repulsive social forces between the individual a and other road users b , which prevents them from approaching each other closely. $\mathbf{F}_{a,B}$ are repulsive forces of delimiting infrastructure and $\mathbf{F}_{a,i}$ are attractive forces between persons that lead to group formation or draw people towards points of interest. For the scope of this publication, we only consider the destination force and repulsive forces of other road users. It is straightforward to add the other forces in future developments. Negative resulting forces are treated as 0.

The definition of the social force as an acceleration is suitable for particles that can be accelerated in all directions. The movement of a bicycle, however, is laterally constrained by its two-wheeler characteristics and the necessity to steer to achieve lateral acceleration. The social force can't move the bicycle directly. We, therefore, propose a reformulation of the social force that describes the intended velocity vector \mathbf{v}_a rather than an acceleration. This may then be used as input for our controlled dynamic bicycle model.

$$\mathbf{F}_a := \mathbf{v}_a \quad (5)$$

As a result, the social *force* is now a velocity vector field. This weakens the original analogy with Newtonian forces. However, when used as the input of a controlled dynamic system, it retains its interpretability as the motivation to act. It is the desired quantity that the control system follows. To keep the reference to its origin, we retain the name *social force*. Zhao et al. (2023) have previously successfully applied similar velocity force fields as cost functions for the simulation of car interactions with optimal control.

Destination Force

Helbing and Molnár (1995) designed the destination force to point in the direction that corrects an agent's movement from its current velocity vector to the preferred velocity vector. Huang et al. (2012) use the same approach for their social force model for cars. This introduces a feedback loop that controls the agent to move in the direction of the desired destination. More complex dynamic models, however, may require dedicated tunable controllers to be stabilized and follow a desired trajectory. Hence, we propose to reformulate the destination force. To be used as an input for the controlled dynamic model, the destination force should directly point toward where the agent wants to go. This may either be a vector pointing at a desired location or a vector following a desired path. If the destination force directly points towards the desired destination, discontinuities occur when the bicycle has reached a destination and the force vector jumps to the next destination in the desired path or guideline proposed by Kath (2023). These

jumps can lead to instability of our dynamic model. Instead, we calculate the destination force based on a smooth spline connecting multiple intermediate locations. Let $\mathbf{p}_1^0 \dots \mathbf{p}_i^0$ be a series of i consecutive destinations ahead of the cyclist and \mathbf{p}_t^a the position of a cyclist a at time t . Then, $\mathbf{p}_1^s \dots \mathbf{p}_j^s$ are j points of a B-spline $\gamma(t)$ through $\mathbf{p}_{t-\mu}^a, \mathbf{p}_t^a, \mathbf{p}_1^0 \dots \mathbf{p}_i^0$. The look-back offset μ is a small multiple of the sampling time to include a previous location from the bike's trajectory, smoothing the spline at the bike's current orientation. The destination force then points in the direction

$$\mathbf{e}_{F0} = \frac{\mathbf{p}_{1+\nu}^s - \mathbf{p}_1^s}{\|\mathbf{p}_{1+\nu}^s - \mathbf{p}_1^s\|}, \tag{6}$$

where ν describes a look-ahead offset to compensate for the delay introduced by the dynamic bicycle model. While going straight, the magnitude of the destination force is given by the velocity v_d that the cyclist desires. For turns, we derive $\|\mathbf{F}^0\|$ from the curvature of the spline ahead of the cyclist, given as (Pressley, 2010, p. 31)

$$\kappa = \frac{\|\ddot{\gamma} \times \dot{\gamma}\|}{\|\dot{\gamma}\|^3} = \frac{|\dot{\gamma}_x \ddot{\gamma}_y - \dot{\gamma}_y \ddot{\gamma}_x|}{\sqrt{\dot{\gamma}_x^2 + \dot{\gamma}_y^2}^3}, \tag{7}$$

where $\gamma(t) = (\gamma_x(t), \gamma_y(t), 0)^T$ is the spline in the xy-plane and a dot denotes the derivative $\frac{d}{dt}$. Interpreting the curvature as the inverse of the turn radius $R = \frac{1}{\kappa}$, we may then use the following relationship given by Karnopp (2013, p.152) to determine the radius of a turn at a constant speed and roll angle:

$$R = \frac{v^2}{g\theta_{ss}}. \tag{8}$$

This is derived from the steady state roll angle θ_{ss} at a constant steer angle and the geometric relationship between steer angle and turn radius. Assuming that riders unconsciously choose a maximum comfortable roll angle $\theta_c = \theta_{ss}$ for their maneuvers, this gives the ideal speed for a turn of radius R . It serves as a turn-dependent upper limit to the destination force otherwise equaling the preferred cycling speed v_d . Additionally, we introduce a lower speed limit v_s that prevents the destination force from suggesting unstable speeds for small turn radii. The final expression of the destination force magnitude is:

$$\|\mathbf{F}^0\| = v(\kappa) = \begin{cases} v_s & \text{if } \sqrt{g\frac{\theta_c}{\kappa}} < v_s \\ v_d & \text{if } \sqrt{g\frac{\theta_c}{\kappa}} > v_d \\ \sqrt{g\frac{\theta_c}{\kappa}} & \text{otherwise} \end{cases}. \tag{9}$$

Repulsive Forces

In the social force model, repulsive forces prevent road users from approaching each other closely. Generally, the magnitude of these forces describes how strong an opponent reacts, while the direction of the repulsive force describes the direction of any evasive maneuver. For a pair of cyclists, these realistic reactions depend on their relative position and relative orientation. For example, two cyclists going parallel to each other might be comfortable with a small lateral clearance that only requires minor evasive action, whereas encroaching maneuvers might require strong breaking and steering to prevent collisions. We directly tailor repulsive force fields $\mathbf{F}_{rep,a,b} = F_{rep,a,b} \cdot \mathbf{e}_{rep,a,b}$ to represent this anisotropy of cyclist interactions. For convenience, the relative position of two cyclists a and b is expressed in polar coordinates $(r_{a,b}, \varphi_{a,b})$ centered at a 's position. $\psi_{a,b}$ is their relative heading. Similar to Helbing and Molnár, we base the contour lines of our force field on ellipses described by

$$r_{a,b}(\varphi_{a,b}) = \frac{\beta}{\sqrt{1 - (e(\psi_{a,b}) \cos \varphi_{a,b})^2}}, \tag{10}$$

where β is the semi-minor axis of the ellipse and $e(\psi_{a,b})$ is an anisotropic eccentricity. Additionally, we introduce an anisotropic radial decay $\sigma(\varphi_{a,b}, \psi_{a,b})$. The magnitude of repulsive force then becomes

$$F_{rep,a,b}(r_{a,b}, \varphi_{a,b}) = F_0 \exp\left(-\frac{\beta}{\sigma(\varphi_{a,b}, \psi_{a,b})}\right) = F_0 \exp\left(-\frac{r_{a,b} \sqrt{1 - (e(\psi_{a,b}) \cos \varphi_{a,b})^2}}{\sigma(\varphi_{a,b}, \psi_{a,b})}\right). \tag{11}$$

The direction of the repulsive force is perpendicular to the contour lines and hence equals the direction of the negative gradient:

$$e_{\text{rep},a,b} = -\frac{\nabla F_{\text{rep},a,b}(r_{a,b}, \varphi_{a,b})}{\|\nabla F_{\text{rep},a,b}(r_{a,b}, \varphi_{a,b})\|} \quad (12)$$

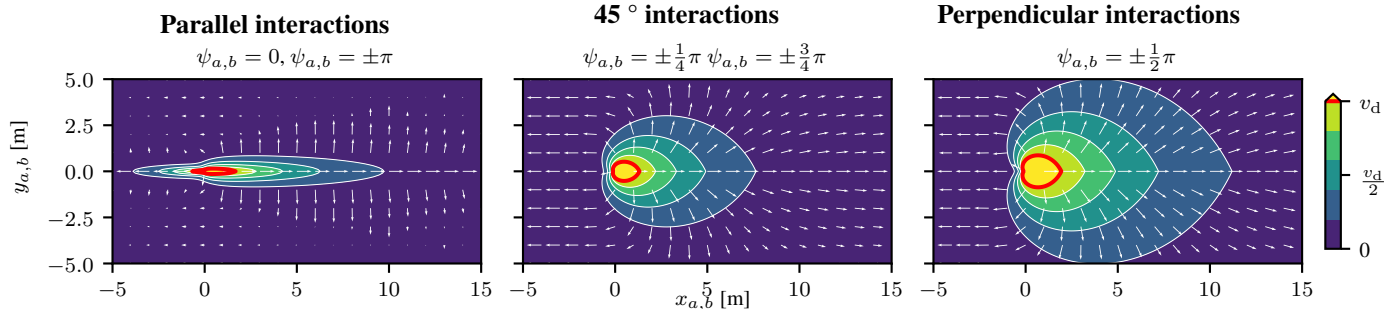


Figure 3. Repulsive force acting on a cyclist b interacting with a cyclist a (located at $(0, 0)$, riding in x -direction) for different relative orientations $\psi_{a,b}$ and positions $(x_{a,b}, y_{a,b})$. Colors indicate the magnitude of the force field as multiples of the desired velocity v_d of b . At the red line, the repulsive force equals the maximum of b 's destination force. The force direction (black arrows) experienced by b is perpendicular to the contour lines. Parameter values: $F_0 = 7 \frac{\text{m}}{\text{s}}$, $e_0 = 0.995$, $e_1 = 0.7$, $\sigma_0 = 0.5 \text{ m}$, $\sigma_1 = 5.0 \text{ m}$, $\sigma_2 = -0.3 \text{ m}$, $\sigma_3 = -4.9 \text{ m}$.

We introduce the two anisotropic properties to enable passing with small lateral clearances for parallel interactions and early braking for perpendicular interactions. In the first case, the contour lines of the force field should be elongated in the cyclist's direction of travel and narrowed perpendicular to this direction. In the second case, the contour lines must approach a circular shape and have a low radial decay to ensure early reaction. In both cases, the area in front of the cyclists must have strong repulsive forces with a small radial decay to prevent collisions. The area behind the cyclists may have large radial decay to allow others to follow closely. To achieve these properties, we modulate the eccentricity and decay as follows:

$$e(\psi_{a,b}) = e_0 - e_1 \sin^2 \psi_{a,b} \quad (13)$$

$$\sigma(\varphi_{a,b}, \psi_{a,b}) = \sigma_0 + \sigma_1 \sin^2 \psi_{a,b} + (\sigma_2 + \sigma_3 \sin^2 \psi_{a,b}) \left| \sin \frac{\varphi_{a,b}}{2} \right| \quad (14)$$

This introduces the tune-able parameters $0 < e_1 < e_0 < 1$, $\sigma_0, \sigma_1 > 0$, $\sigma_2 > -\sigma_0$, and $\sigma_3 > -\sigma_1$. Figure 3 shows the resulting almond-shaped force fields for different relative orientations between two cyclists a and b . We chose these modulation functions heuristically to create force fields with the properties described above. Hence, they are not unique and do not guarantee optimal performance.

Control Architecture

To make a simulated cyclist a execute the movement indicated by the overall social force F_a , we introduce two separate control loops for speed and yaw (see Figure 1). The first system controls the speed v based on social force magnitude $v_d = \|F_a\|$ experienced by a . The second system controls the yaw angle ψ based on the desired yaw derived from the social force angle $\psi_d = \angle F_a$.

Roll and Yaw Angle Control

When riding a bicycle, humans try to reach their destination while also having to keep the bicycle stable. We describe this effort with a nested control loop for the roll angle $\theta(t)$ and yaw angle $\psi(t)$ (Figure 4). Firstly, a PI-controller derives the desired roll angle from the yaw error. The desired roll angle is the input for the inner loop, which consists of a D-controller that derives the torque $\tau(t)$ at the handlebar, the steer column dynamics $G_\delta(s)$, and the roll dynamics $G_\theta(s)$. Note that ideal D-characteristics are not realizable for physical systems. However, in our simulation scenario, the transfer function of the inner loop still retains a higher

degree denominator than numerator and hence is realizable as a whole. One may also interpret the inner loop as the combined human roll control dynamics and implement this for simulation. The inner loop transfer function with respect to the roll angle θ is

$$G_{\text{inner},\theta}(s) = \frac{\Theta(s)}{\Theta_d(s)} = \frac{G_{R2}(s)G_\delta(s)G_\theta(s)}{1 + G_{R2}(s)G_\delta(s)G_\theta(s)} = \frac{-KK_D\tau_2s - KK_D}{I\tau_1^2s^3 + c\tau_1s^2 - (I + KK_D\tau_2)s - (c + KK_D)}. \quad (15)$$

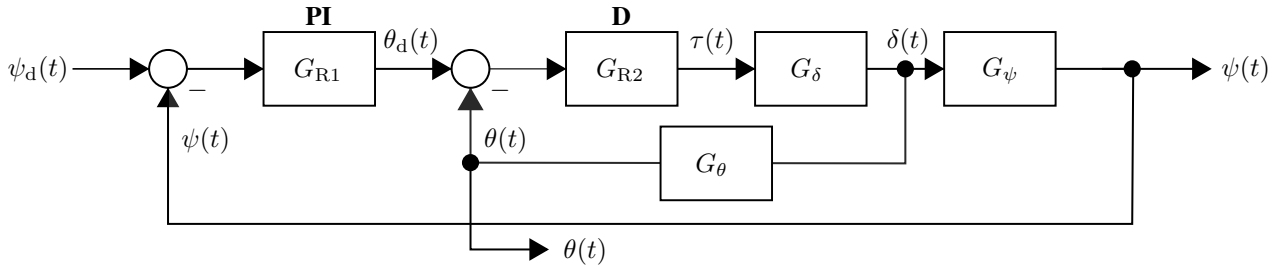


Figure 4. Nested control of steer $\delta(t)$ and yaw $\psi(t)$.

Using the Routh–Hurwitz stability criterion, four stability conditions for the inner loop can be derived:

$$(A_2) \quad K_D < -\frac{I_s}{K\tau_2} = -\frac{I_s gl}{l_2 v} \quad (A_3) \quad K_D < -\frac{c}{K} = -\frac{cgl}{v^2} \quad (B_{1-1}) \quad K_D < 0 \quad (B_{1-2}) \quad v < \frac{cl_2}{I_s} \quad (16)$$

For a realistic moment of inertia $I_s < 1$ of the steering column, realistic steering dampening $c \gg 1$, bike dimensions $l_1 \approx 1$, and realistic speed $v < 15 \frac{m}{s}$, (A_2) is dominated by (A_3) and (B_{1-2}) is always satisfied. The inverse dependency on the bicycle speed means that no bounded gain K_D will be able to stabilize the bicycle at all speeds. For very small speeds, the average cyclist has to step off the bike to prevent falling. This minimum speed for stability can be tuned by choosing a suitable K_D . We create an adaptive $K_D(v)$ that enables stability at low speeds while preventing unreasonably large controller outputs at higher speeds. With

$$K_D(v) = \frac{k_{d0}}{v + k_{d1}}, \quad (17)$$

instability of the inner loop occurs for $v < \frac{-cgl - \sqrt{(cgl)^2 - 4cglk_{d0}k_{d1}}}{2k_{d0}} \approx 0.98 \frac{m}{s}$. Figure 5 shows (16) - (17) for the values of a common bike (Moore, 2015).

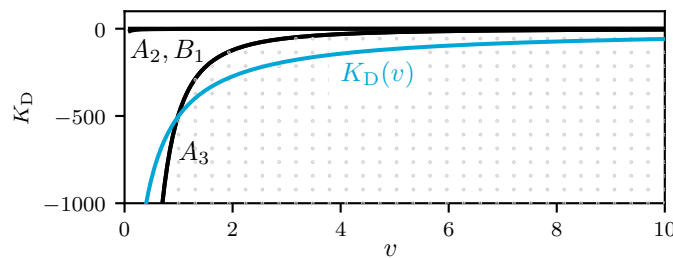


Figure 5. Stability limits (black lines) and stability region (gray dots) of the inner loop for $K_D(v)$ with $k_{d0} = -600$, $k_{d1} = 0.2$, $I_s = 0.07 \text{ kgm}^2$, $c = 50 \text{ Nms}$.

The outer loop takes the steer angle from the inner loop and passes it to the steer-yaw transfer function $G_\psi(s)$:

$$G_{\text{outer}}(s) = \frac{\Psi(s)}{\Psi_d(s)} = \frac{G_{R1}(s)G_{\text{inner},\delta}(s)G_\psi(s)}{1 + G_{R1}(s)G_{\text{inner},\delta}(s)G_\psi(s)} = \frac{b_2s^3 + b_3s^2 + b_4s + b_5}{a_0s^5 + a_1s^4 + a_2s^3 + a_3s^2 + a_4s + a_5}. \quad (18)$$

with $G_{\text{inner},\delta}(s) = \frac{\Delta(s)}{\Theta_d(s)} = \frac{G_{\text{inner},\theta}}{G_\theta(s)}$ and the parameters:

$$\begin{aligned} a_0 &= I\tau_1^2\tau_3 & a_2 &= (K_P K_D \tau_1^2 - (I + K K_D \tau_2)\tau_3) & a_4 &= -K_P K_D \\ a_1 &= c\tau_1^2\tau_3 & a_3 &= (K_I K_D \tau_1^2 - (c + K K_D)\tau_3) & a_5 &= -K_I K_D \end{aligned} \quad (19)$$

$$b_2 = K_P K_D \tau_1^2 \quad b_3 = K_I K_D \tau_1^2 \quad b_4 = -K_P K_D \quad b_5 = -K_I K_D \quad (20)$$

Again, we evaluate the Routh–Hurwitz stability criterion to find limits for the gain parameters. The symbolic expressions of the stability conditions based on Routh coefficients of the fifth-order system are very long. For brevity, we only present their numerical solutions (Fig. 6) using the inner loop gain and bicycle parameters from above (Fig. 5).

Figure 6 illustrates that speed-adaptive outer loop gains have little effect on the stability range. We choose K_P and K_I to be constant to limit the number of model parameters. The minimum stable speed results from the intersection of the stability limit D_1 and the gain curves. Numerically, we determine $v_{\min} \approx 2.26 \frac{m}{s}$. This is notably higher than the minimum stable speed of the inner loop (Fig. 5). Within the scope of this paper, we intend to do experiments at normal riding speeds ($3 - 6 \frac{m}{s}$). Hence, the stability range is sufficient.

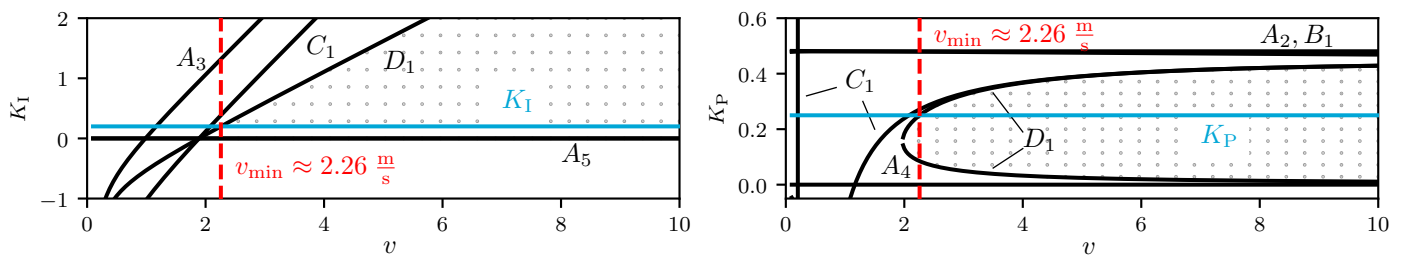


Figure 6. Stability limits (solid black) and stable area (gray dots) of the outer loop for the gains $K_P = 0.25$ and $K_I = 0.2$. Capital letters naming the constraints refer to the corresponding coefficients of the Routh table.

Speed

For simplification, the inverted pendulum bicycle model assumes constant speed. However, simulated cyclists need to adapt their speed $v(t)$ according to the magnitude of experienced social force $v_d(t) = \|\mathbf{F}_a\|$. Hence, we introduce a second independent control loop for the speed. This loop (Figure 7) consists of a P-controller to derive an acceleration from the current speed error and an integrator to model the bicycle speed. For simplicity, this controller implicitly incorporates driving forces, friction, and drag. We set conservative limits ($-3 \frac{m}{s^2} \leq a(t) \leq 1 \frac{m}{s^2}$) to prevent unrealistically high acceleration. The resulting longitudinal speed variations violate the above-mentioned assumption of constant speed. However, for sufficiently small simulation time steps and accelerations, the speed variations per step are small as well and may be neglected. Furthermore, Limebeer and Sharma (2008) have previously determined that lateral bicycle dynamics are only little affected by small longitudinal accelerations. This further justifies treating our model as time-invariant. Empirically, we have not observed instability of the roll and yaw angle control due to speed variation.

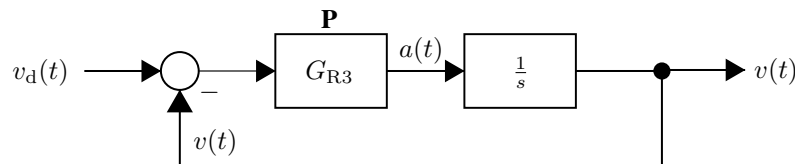


Figure 7. Speed control.

Simulation Results

To demonstrate our model with reformulated social forces and bicycle dynamics, we implement it in Python 3.11 (Python Software Foundation, Beaverton, USA) using the Python Control Systems Library (Fuller et al., 2021) and perform a series of tests. First, we present the desired yaw step response of a single cyclist. Then, we show simulations of multiple cyclist interactions. We compare the results for the inverted pendulum bicycle model and a traditional 2D bicycle model that consists only of a two-dimensional two-wheeler model in the ground plane without consideration of the roll angle (Corke, 2017, p. 101). In a simple control loop, a

P-controller aligns the steering angle with the desired yaw angle. Other than that, the 2D bicycle model shares the embedding of the inverted pendulum model into the cyclist social force model, including spline-based destination forces and repulsive force fields.

For this demonstration, we use the physical parameters of a standard bicycle, $l_1 = l_2 = 0.5$ m, $h = 1$ m, $m = 87$ kg, $I_b = 3.28 \frac{\text{kg}}{\text{m}^2}$, presented by Moore (2015). We tune the steer column dynamics heuristically to produce the expected outcome. The resulting values are $I_s = 0.07$ kgm² and $c = 50.0$ Nms. For full calibration, these values need to be experimentally confirmed. Similarly, we heuristically calibrate the cyclist social force and control parameters so that the simulation shows the expected effects. Figures 3, 5, and 6 list their values. We choose the comfortable roll as $\theta_c = 10^\circ$ and simulated cyclists ride at desired velocities of $3 - 6 \frac{\text{m}}{\text{s}}$. A calibration based on naturalistic driving data was not possible due to the unavailability of suitable data at the current time.

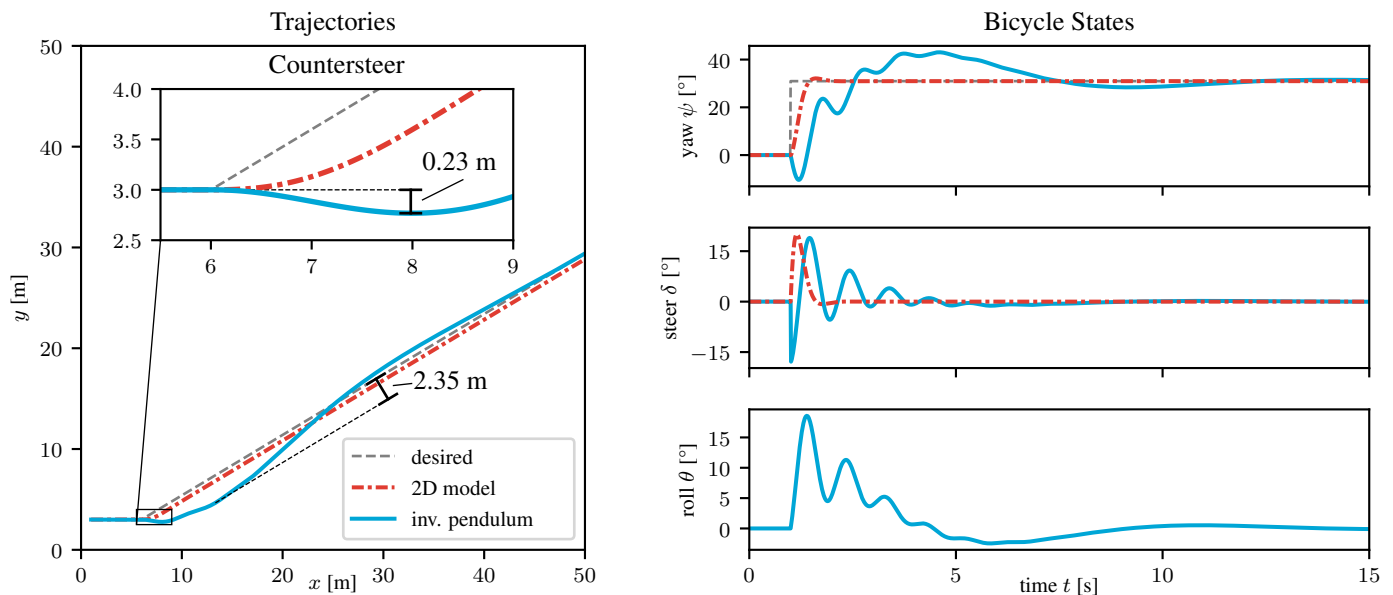


Figure 8. Yaw angle step response at constant speed. Comparison between the inverted pendulum bicycle dynamics (solid blue) and 2D bicycle dynamics (dash-dotted red). The left column shows the simulated trajectories with the reaction to a sudden change of the desired yaw angle. The right column shows the simulated bicycle states over time.

In the first experiment, we apply a step in the desired yaw angle to a cyclist traveling at constant speed. To get an undisturbed view of the yaw and roll dynamics, we disable path planning and adaptive speed for this scenario. Figure 8 shows the trajectories of an inverted pendulum and a 2D bicycle (left column) together with the corresponding yaw, steer, and roll angles over time (right column). The step of the desired yaw angle to the left leads to a steep rise of steer angle in the opposite direction to initiate the turn. Steering to the right makes the inverted pendulum cyclist (solid blue) fall left into the intended turn. With the roll angle in the right direction, the controller then quickly steers to the left to perform a left turn. This showcases the countersteering effect that is necessary to control a bicycle. An enlarged part of the trajectory plot focuses on the moment when the yaw angle step is applied to visualize the countersteering effect. The inverted pendulum cyclist notably swerves to the right, whereas the 2D cyclist directly steers left. This leads to a lateral displacement of approximately 23 cm (see inset of Figure 8). The maneuver also results in a delay between the desired and actual change of direction, which the inverted pendulum bike only slowly recovers from. At its maximum, it laterally diverts 2.35 m from the ideal step response trajectory. The oscillations of the yaw angle also show how the inverted pendulum cyclist has to use lateral motion to stabilize the bike while trying to execute the desired maneuver. On the other hand, the 2D bicycle (dash-dotted red) follows the sudden change in direction faster, without a swerve in the other direction and with a smaller lateral offset.

In a second experiment, we create four scenarios for our simulated cyclists. This time, the whole model pipeline is active, including path planning for destination force calculation and adaptive speeds. The model parameters in all four scenarios are identical to the first experiment. The left column of Figure 9 shows a snapshot of the simulation with one or more inverted pendulum cyclists. It visualizes the cyclists' trajectories up to that moment, the planned path, the social forces acting on the cyclist at that moment, and any intermediate destinations of the cyclist. The right column presents the final trajectories of the inverted pendulum bike (solid blue) and the 2D bike (dash-dotted red). In the 'parcours' scenario, a single cyclist has to travel to a series of destinations with lateral offset

to demonstrate the model’s agility. Both cyclist models execute the curves given by the intermediate destinations. Similar to the step response experiment, the inverted pendulum cyclist is lagging behind due to the delay introduced by the need to countersteer. Note that, in our simulation, the cyclists don’t have to reach an intermediate destination fully. After a cyclist has approached a destination closer than the distance $d_{min} = 2$ m, they switch to the next.

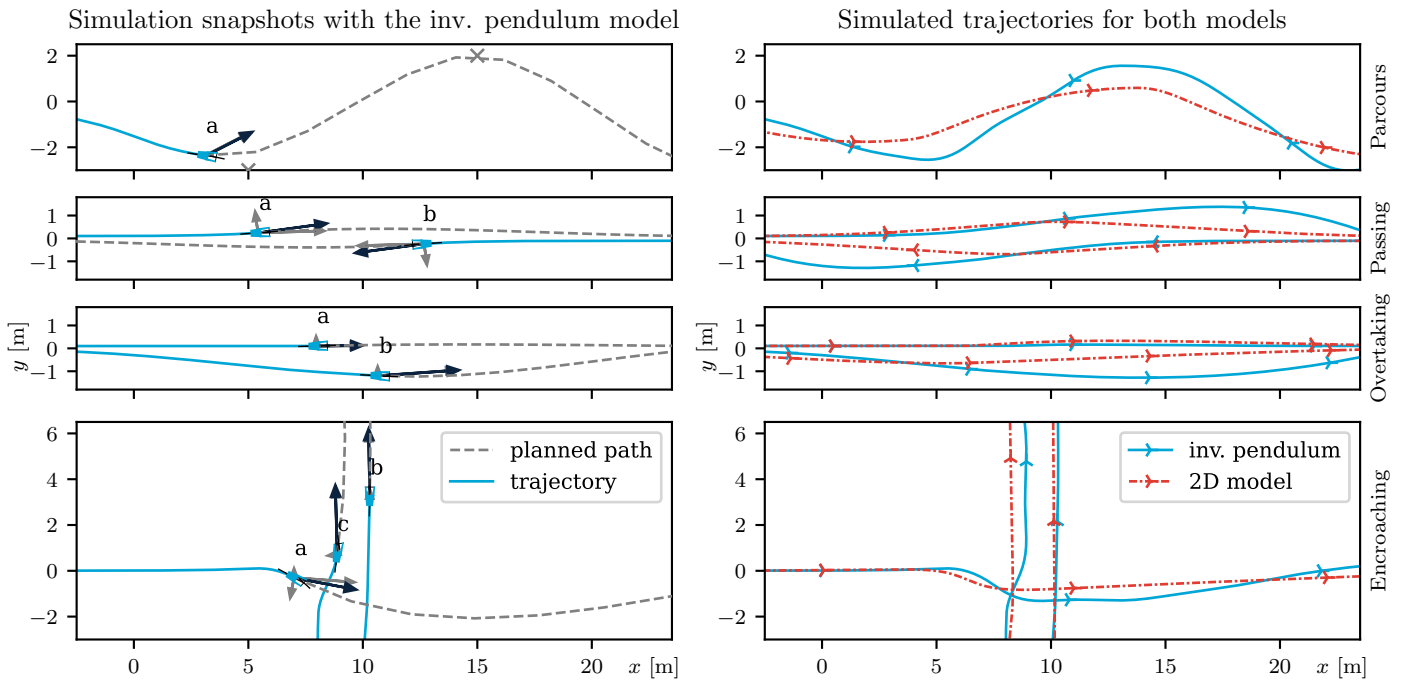


Figure 9. Simulations of interaction test scenarios (top to bottom: ‘parcours’, ‘passing’, ‘overtaking’, ‘encroaching’). The left shows simulation snapshots of inverted pendulum bikes during interaction. Arrows indicate the individual social forces experienced by the cyclist (gray) and the resulting force (dark blue). The right compares the simulated trajectories of inverted pendulum bikes (solid blue) and 2D bikes (dash-dotted red).

The other three scenarios show simple interactions of multiple cyclists to demonstrate the general capability of our model to handle common interactions. In the ‘passing’ and ‘overtaking’ scenarios, two interactions are shown. Two cyclists evade each other smoothly and the trajectories of the 2D and inverted pendulum models show only small differences at the beginning of each maneuver. Again, countersteering causes a delay in the reaction of the inverted pendulum cyclists, but the effect is small because the desired course correction is only very minor. In the second half of the maneuvers, the two model variants differ more. In the absence of any repulsive forces after the cyclists have passed each other, the path-planning-based destination force is the only influencing factor. Re-planning the path to the destination in every time step amplifies the small lag of the inverted pendulum bicycle compared to the 2D bicycle. The return to a straight path becomes unrealistically wide and delayed. The fourth scenario (‘encroachment’) shows an interaction of three cyclists. In an evasive maneuver, the two cyclists traveling upwards slightly swerve to the right, while the single cyclist traveling right decelerates and performs a stronger evasive maneuver. Again, the inverted pendulum bikes show a small lag in their trajectory and small decaying oscillations after the initial evasive movement. Additionally, Figure 10 shows the lateral deviation of cyclist *a* from the undisturbed straight horizontal trajectory that both models were tasked with. The evasive maneuver of the inverted pendulum cyclist results in more than a 1 m bend to the right, whereas the 2D cyclist requires about 40 cm less lateral space. This puts into numbers how the additional need to stabilize the bike affects the space requirements.

Lastly, we report the Post-Encroachment Time (PET), which measures the time between the first bicycle leaving and the second bicycle entering the conflict area and is a surrogate safety indicator designed to assess the safety of road user interactions (Allen et al., 1978). For simplicity, we calculate the PET with respect to the intersection of the trajectories of the road user center points and do not consider their footprint. Table 1 shows a difference of more than 11% between the two models for the interaction of *a* and *b*. This shows that the inverted pendulum model notably affects typical performance measures used in traffic simulation and assessment.

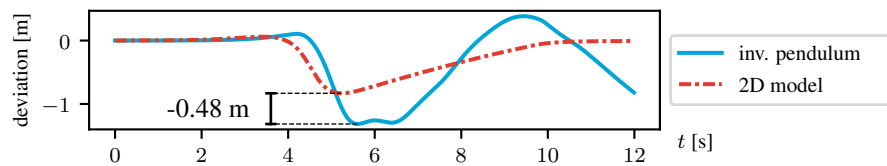


Figure 10. Deviation of cyclist *a* in the 'encroaching' scenario from its undisturbed path.

Table 1. Post Encroachment Times (PET) in the 'encroaching' scenario of Figure 9 for both model types.

bike models	PET between <i>a</i> and <i>b</i>	PET between <i>a</i> and <i>c</i>
inv. pendulum	1.86 s	1.00 s
2D model	1.64 s	0.93 s

Discussion

The test scenarios show the general capability of the social force reformulation and the inverted pendulum model to describe cyclist interactions. Compared to established microscopic frameworks, this enables lane-free simulation of road user interactions. Additionally, the simulated trajectories of our model exhibit countersteering and lateral oscillation for stabilization. Compared to the 2D model without roll angle, these affect the relative positions, orientations, and speeds of the cyclists. The PET measurements demonstrate that this can result in notable differences of typical performance indicators and hence might lead to a different assessment of an interaction. Furthermore, we observe that the need to stabilize the bicycle leads to an increase in space requirements. For example, a lateral countersteering displacement of 23 cm corresponds to 10 % of the width of a unidirectional Dutch bicycle path (Veroude et al., 2022). Similarly, the lateral deviation difference between the inverted pendulum model and the 2D model is 48 cm or 20.1 % of the width of a Dutch bicycle lane (Veroude et al., 2022). These results show that the stabilization task impacts cyclists' reactions to disturbances in a way relevant to simulation applications like infrastructure design and safety assessment. Qualitatively, the underlying physics support the behavior of our model. Quantitatively, heuristic parameter value choice without calibration based on real-world data limits the interpretability of the observed effect magnitude. While we plan to perform calibration and validation in our next work, the presented simulations seem realistic. For example, the step response leads to a countersteering motion of about 2 m in length at a speed of $5 \frac{\text{m}}{\text{s}}$, which equates to a countersteering duration of 0.4 s. Therefore, these first results strengthen our hypothesis that more realistic bicycle dynamics are significant for the micro-simulation of bicycle interactions.

Shortcomings of the model are apparent in the unrealistic course corrections after the interaction in the 'overtaking' and 'passing' scenarios. This effect is created by our spline-based path planning. More advanced path planners or predictive control may solve the issue. Other shortcomings relate to missing functionalities of a full interaction model. These are, for example, coming to a halt at a specific location or identifying a crash from large roll angles. For the first case, the model already creates a minimum speed at which the bicycle becomes unstable. To perform experiments in the critical speed range, tuning of the controller enables calibrating the slow-speed stability. The transition between riding and a safe and accurate stop is yet unsolved.

Conclusion

In this work, we present how physics-based bicycle dynamics may influence the microscopic simulation of cyclists. Firstly, our cyclists are constrained by the degrees of freedom available to a two-wheeler. Secondly, we add the simulation of the roll angle to the bicycle, which introduces countersteering and lateral oscillation for stabilization. In a comparison of simulated bicycle trajectories with and without roll angle, this notably impacts the simulated maneuvers in terms of lateral deviation and post-encroachment time. Hence, simulating bicycle dynamics may affect an assessment of interactions on a microscopic level and the aggregated performances on a macroscopic level.

To enable the coupling between the social force model and a bicycle dynamics model, we present a reformulation of the social force model. This interprets the social force as a desired velocity rather than an acceleration. The desired velocity vector then becomes the input of our controlled bicycle model. A new spline-based destination force pointing directly along the desired path decouples

the social force model and the control of the bicycle dynamics. Additionally, we tailor anisotropic force fields to describe the largely anisotropic characteristics of bicycle traffic. We heuristically arrive at these design choices motivated by the creation of a model that showcases the known real-world effects described above. Going further, we plan to calibrate and validate our model based on real-world data to confirm the hypothesis that realistic bicycle dynamics are an important element of simulated interactions.

References

- Allen, B. L., Shin, B. T., and Cooper, P. J. (1978). Analysis of traffic conflicts and collisions. *Transportation Research Record*, 667(1):67–74.
- Arun, A., Haque, M. M., Bhaskar, A., Washington, S., and Sayed, T. (2021). A systematic mapping review of surrogate safety assessment using traffic conflict techniques. *Accident Analysis & Prevention*, 153:106016.
- Corke, P. (2017). *Robotics, Vision and Control: Fundamental Algorithms In MATLAB®*, volume 118 of *Springer Tracts in Advanced Robotics*. Springer, Cham, 2nd edition.
- Dias, C., Nishiuchi, H., Hyoudo, S., and Todoroki, T. (2018). Simulating interactions between pedestrians, segway riders and cyclists in shared spaces using social force model. *Transportation Research Procedia*, 34:91–98.
- Fuller, S., Greiner, B., Moore, J., Murray, R., van Paassen, R., and Yorke, R. (2021). The python control systems library (python-control). In *60th IEEE Conference on Decision and Control (CDC)*, pages 4875–4881. IEEE.
- Helbing, D. and Molnár, P. (1995). Social force model for pedestrian dynamics. *Physical Review E*, 51(5):4282–4286.
- Huang, W., Fellendorf, M., and Schönauer, R. (2012). Social Force based Vehicle Model for 2-dimensional Spaces. In *Transportation Research Board 91st Annual Meeting*, Washington D.C. Transportation Research Board.
- Karnopp, D. (2013). *Vehicle Dynamics, Stability and Control*. Mechanical Engineering. CRC Press, Boca Raton, 2nd edition.
- Kaths, H. (2023). A movement and interaction model for cyclists and other non-lane-based road users. *Frontiers in Future Transportation*, 4.
- Kaths, H., Keler, A., and Bogenberger, K. (2021). Calibrating the Wiedemann 99 Car-Following Model for Bicycle Traffic. *Sustainability*, 13(6):3487.
- Kurtc, V. and Treiber, M. (2020). Simulating bicycle traffic by the intelligent-driver model-Reproducing the traffic-wave characteristics observed in a bicycle-following experiment. *Journal of Traffic and Transportation Engineering (English Edition)*, 7(1):19–29.
- Liang, X., Xie, M., and Jia, X. (2018). New Microscopic Dynamic Model for Bicyclists' Riding Strategies. *Journal of Transportation Engineering, Part A: Systems*, 144(8):04018034.
- Limebeer, D. J. N. and Sharma, A. (2008). The dynamics of the accelerating bicycle. In *2008 3rd International Symposium on Communications, Control and Signal Processing*, pages 237–242.
- Moore, J. K. (2015). *Bicycle Control Design in Python/v3*. Plotly, Montreal, <https://plotly.com/python/v3/ipython-notebooks/bicycle-control-design/>.
- Ni, Y., Li, Y., Yuan, Y., and Sun, J. (2023). An operational simulation framework for modelling the multi-interaction of two-wheelers on mixed-traffic road segments. *Physica A: Statistical Mechanics and its Applications*, 611:128441.
- Pressley, A. (2010). *Elementary Differential Geometry*. Springer Undergraduate Mathematics Series (SUMS). Springer, 2 edition.
- Rinke, N., Schiermeyer, C., Pascucci, F., Berkhahn, V., and Friedrich, B. (2017). A Multi-layer Social Force Approach to Model Interactions in Shared Spaces Using Collision Prediction. *Transportation Research Procedia*, 25(1):1249–1267.
- Veroude, B., Gulp, M. v., and Boggelen, O. v. (2022). *Geactualiseerde aanbevelingen voor de breedte van fietspaden 2022*. Fietsberaad CROW, <https://www.fietsberaad.nl/Kennisbank/Aanbevelingen-breedte-fietspaden-2022>.
- Yuan, Y., Goñi-Ros, B., van Oijen, T. P., Daamen, W., and Hoogendoorn, S. P. (2019). Social Force Model Describing Pedestrian and Cyclist Behaviour in Shared Spaces. In *Traffic and Granular Flow '17*, pages 477–486, Cham. Springer.
- Zhao, J., Knoop, V. L., and Wang, M. (2023). Microscopic traffic modeling inside intersections: Interactions between drivers. *Transportation Science*, 57(1):135–155.